Supporting Information for "Pathways of Nitrous Oxide Production in the Eastern Tropical South Pacific Oxygen Minimum Zone"

Daniel McCoy[1], Pierre Damien[1], Daniel Clements[1], Simon Yang[1], Daniele

Bianchi[1]

[1]Department of Atmospheric and Oceanic Sciences

[1]University of California – Los Angeles

[1]520 Portola Plaza, Los Angeles, CA 90095, USA

Contents of this file

1. Text S1 to S4

   - S1: Treatment of Organic Matter

   - S2: NitrOMZ Nitrogen Cycle

   - S3: NitrOMZ Tracer Sources-and-sinks

   - S4: Light Inhibition

2. Tables S1 to S5

3. Figures S1 to S14

————

Corresponding author: Daniel McCoy, Department of Atmospheric and Oceanic Sciences, University of California – Los Angeles, 520 Portola Plaza, Los Angeles, CA 90095, USA. (demccoy@atmos.ucla.edu)

December 7, 2022, 8:52pm

S1: Treatment of Organic Matter In the model, remineralization of sinking particulate OM follows the formulation of Moore, Doney, and Lindsay (2004), where sinking is implicit and based on the ballast model from Armstrong, Lee, Hedges, Honjo, and Wakeham (2001). Particulate organic carbon (POC) in BEC is produced at each time-step following:

$$R_{prod}^{poc}(z) = (R_{graze,poc}^{sp}(z) + R_{graze,poc}^{diat}(z) + R_{graze,poc}^{diaz}(z)) + (R_{agg}^{sp}(z) + R_{agg}^{diat}(z) + R_{agg}^{diaz}(z)) +$$

$$(R_{loss,poc}^{sp}(z) + R_{loss,poc}^{diat}(z) + R_{loss,poc}^{diaz}(z)) + f_{zoo}^{d} R_{zoo}^{l}(z).$$

See Table S1 for descriptions of each rate; further details can be found in Deutsch et al. (2021). POC production is then partitioned into a free and mineral component:

$$R_{prod}^{poc}(z) = R_{prod}^{free,poc}(z) + R_{prod}^{min,poc}(z). \tag{1}$$

Following equation (1), both free and mineral POC is instantaneously distributed in the water column following one-dimensional steady-state production-remineralization equations. The vertical profile of free POC flux (Φ_{poc}) is calculated as:

$$\Phi_{free,poc}(z) = \Phi_{free,poc}(z_o)e^{-\frac{1}{\lambda_{poc}}(z-z_o)} + \int_{z_o}^{z} R_{free,poc}^{prod}(z)e^{-\frac{1}{\lambda_{poc}}(z-z_o)}dz. \tag{2}$$

Here, λ_{poc} is a discretized exponential scale length computed from an initial scale length (γ_{poc}) that is modified by both the local O_2 concentration of layer z:

$$\gamma_{poc} = \begin{cases} \gamma_{poc} * 3.3 & \text{where } O_2 < 5 \text{ mmol/m}^3 \\ \gamma_{poc} * (1 + (3.3 - 1)(40 - o_2)/35) & \text{where } 5 \text{ mmol/m}^3 < O_2 < 40 \text{ mmol/m}^3 \\ \gamma_{poc} & \text{elsewhere} \end{cases} \tag{3}$$

and its thickness dz:

$$\lambda_{poc} = \begin{cases} \gamma_{poc} * (1.0), & \text{where dz} <100\text{m} \\ \gamma_{poc} * (1.0 * (2.9 - 1.0) * (-dz - 1.0)/(2.9 - 1.0), & \text{where } 100\text{m}<\text{dz}<250\text{m} \\ \gamma_{poc} * (2.9 * (5.6 - 2.9) * (-dz - 2.9)/(5.6 - 2.9), & \text{where } 250\text{m}<\text{dz}<500\text{m} \\ \gamma_{poc} * (5.6 * (5.7 - 5.6) * (-dz - 5.6)/(5.7 - 5.6), & \text{where } 500\text{m}<\text{dz}<700\text{m} \\ \gamma_{poc} * (5.7). & \text{elsewhere} \end{cases} \quad (4)$$

See Table S2 for parameter values.

The vertical profile of POC flux for each mineral is calculated as the sum of a soft and hard component (where the hard component is a fraction of the total based on f_{pcaco3}, f_{psio_2}, and f_{dust}, respectively, see Table S2). The soft component for $CaCO_3$, SiO_2, and dust follow similar remineralization processes as in equation (2), whereas the hard components remineralize according to λ_{hard} and $\lambda_{hard,dust}$ (for dust). The fluxes of each mineral are then summed in C units:

$$\Phi_{min,poc}(z) = \rho_{pcaco3}(\Phi^{soft}_{pcaco3}(z) + \Phi^{hard}_{pcaco3}(z)) +$$

$$\rho_{psio_2}(\Phi^{soft}_{psio_2}(z) + \Phi^{hard}_{psio_2}(z)) +$$

$$\rho_{dust}(\Phi^{soft}_{dust}(z) + \Phi^{hard}_{dust}(z))$$

Remineralization at each vertical level is then calculated as the divergence of the POC flux:

$$R^{poc}_{rem}(z) = R^{poc}_{prod}(z) + \frac{d}{dz}(\Phi_{free,poc}(z) + \Phi_{min,poc}(z)) \quad (5)$$

In contrast, dissolved organic carbon (DOC) is an explicit ROMS-BEC tracer and is remineralized (R^{doc}_{rem}) based on a timescale of 15 years with a sharp decrease (6.85%) applied below the euphotic zone as in Frischknecht, Münnich, and Gruber (2017). Local OM remineralization in the water column (R^{tot}_{rem}) is calculated as the sum of POC and DOC remineralization:

$$R^{tot}_{rem}(z) = R^{poc}_{rem}(z) + R^{doc}_{rem}(z). \quad (6)$$

December 7, 2022, 8:52pm

S2: NitrOMZ Nitrogen Cycle The NitrOMZ model expands BEC by including, along with aerobic remineralization (R_{rem}), additional heterotrophic denitrification steps under low-O_2 conditions (Bianchi et al., 2022): NO_3^- reduction (R_{den1}), NO_2^- reduction (R_{den2}), and N_2O reduction (R_{den3}). In order to preserve BEC OM cycle, R_{rem}^{tot} (equation (6)) is partitioned into four possible components at each vertical level and time-step:

$$R_{rem}^{tot}(z) = R_{rem}(z) + R_{den1}(z) + R_{den2}(z) + R_{den3}(z) = \sum_{n=1}^{4} R_i(z), \qquad (7)$$

where i represents one of the four respiration pathways. In practice, we calculate the contribution to total remineralization by each pathway i as:

$$R_i(z) = f_i(z) \cdot R_{rem}^{tot}(z), \qquad (8)$$

where f_i is the relative fraction of remineralization carried out by the process i. The individual depth-dependent fractions are calculated as:

$$f_i(z) = \frac{r_i(z)}{\sum_{i=1}^{4} r_i(z)}, \qquad (9)$$

where r_i is the specific heterotrophic respiration rate of the reaction, calculated based on a maximum remineralization rate modulated by a Michaelis-Menten function of the oxidant utilized (O_2, NO_3^-, NO_2^-, and N_2O for R_{rem}, R_{den1}, R_{den2}, and R_{den3}, respectively) and an exponential inhibition by oxygen (ignored for aerobic respiration):

$$r_i(z) = k_i \cdot \frac{[X](z)}{K_i^X + [X](z)} \cdot e^{-\frac{O_2(z)}{K_i^{o2}}}. \qquad (10)$$

Here, k_i represents the maximum respiration rate for each reaction, K_i^X is the half saturation constant for oxidant $[X]$ uptake, and K_i^{o2} is the scale for inhibition by oxygen.

The chemolithotrophic rates of NH_4^+ oxidation (R_{ao}), NO_2^- oxidation (R_{no}), and anaerobic NH_4^+ oxidation (anammox, R_{ax}) are represented in NitrOMZ using Michaelis-Menten

functions for both the oxidants (O_2, O_2, and NO_2^- for K_{ao}, K_{no}, and K_{ax}, respectively) and reductants (NH_4^+, NO_2^-, and NH_4^+, respectively). The general form for R_{ao} and R_{no} is:

$$R_i(z) = k_i \cdot \frac{[\text{X}](z)}{K_i^X + [\text{X}](z)} \cdot \frac{[\text{Y}](z)}{K_i^Y + [\text{Y}](z)}. \tag{11}$$

Here, k_i represents the maximum respiration rate for each reaction, and K_i^X and K_i^Y are the half saturation constants for oxidant $[X]$ and reductant $[Y]$ uptake, respectively. Both R_{ao} and R_{no} are also inhibited by light, outlined in 1. The rate of anammox follows a similar calculation, but with an additional rate-specific exponential O_2 inhibition (K_{ax}^{o2}) term applied, similar to the heterotrophic denitrification steps in equation (10). See Table S4 for parameter values used in this study.

S3: NitrOMZ Tracer Sources-and-sinks NitrOMZ represents six major components

of the marine nitrogen cycle: N_2, NO_3^-, NO_2^-, N_2O, NH_4^+, and organic nitrogen, which is

linked to POC and DOC via fixed stoichiometry. The biogeochemical sources and sinks

for each of the remaining tracers (in units of $mmol\ m^{-3}$) are:

$$\frac{d}{dt}(N_2) = (Q_{den}^{C:N} \cdot R_{den3}) + R_{ax} + (0.5 \cdot R_{den}^{sed}) \tag{12}$$

$$\frac{d}{dt}(NO_3^-) = R_{no} - (Q_{den}^{C:N} \cdot R_{den1}) - R_{den}^{sed} - R_{up,no_3}^{sp} - R_{up,no_3}^{diat} - R_{up,no_3}^{diaz} \tag{13}$$

$$\frac{d}{dt}(NO_2^-) = R_{ao}^{no2} - R_{no} + Q_{den}^{C:N}(R_{den1} - R_{den2}) - R_{ax} - R_{up,no_2}^{sp} - R_{up,no_2}^{diat} - R_{up,no_2}^{diaz} \tag{14}$$

$$\frac{d}{dt}(N_2O) = 0.5(R_{ao}^{n2o} + (Q_{den}^{C:N} \cdot R_{den2})) - (Q_{den}^{C:N} \cdot R_{den3}) \tag{15}$$

$$\frac{d}{dt}(NH_4^+) = DON(\tau^{DON}) + DONr(\tau^{DONr}) - R_{ao} - R_{ax}$$

$$+ Q_{rem}^{C:N}(R_{loss,dic}^{sp} + R_{loss,dic}^{diat} + R_{loss,dic}^{diaz}) \tag{16}$$

$$+ Q_{rem}^{C:N}(R_{graze,dic}^{sp} + R_{graze,dic}^{diat} + R_{graze,dic}^{diaz} + R_{loss,dic}^{zoo})$$

$$+ Q_{rem}^{C:N}(R_{poc}^{rem}(1 - Q^{DONr})) - (R_{up,nh_4}^{sp} + R_{up,nh_4}^{diat} + R_{up,nh_4}^{diaz}) \tag{17}$$

Here the symbol d/dt denotes the sum of the local time derivative and the physical trans-

port, and $Q_{rem}^{C:N}$ and $Q_{den}^{C:N}$ represent the approximate carbon to nitrogen ratio from rem-

ineralization (16/117) and denitrification (472/2/106), respectively, following Anderson

and Sarmiento (1994). The sedimentary denitrification rate (R_{den}^{sed}) follows the same for-

mulation as in Deutsch et al. (2021).

Following the N_2O tracer and N_2O reduction rate decomposition described in Section

2.4, the equations for each of the N_2O tracers (in units of $mmol\ N_2O\ m^{-3}$) are represented

as:

$$\frac{d}{dt}(\text{N}_2\text{O}_{den}) = Q_{den}^{C:N}(0.5 \cdot R_{den2} - R_{den3}^{den}), \tag{18a}$$

$$\frac{d}{dt}(\text{N}_2\text{O}_{nit}) = (0.5 \cdot R_{ao}^{n2o}) - (Q_{den}^{C:N} \cdot R_{den3}^{nit}), \tag{18b}$$

$$\frac{d}{dt}(\text{N}_2\text{O}_{bou}) = -Q_{den}^{C:N} \cdot R_{den3}^{bou}, , \tag{18c}$$

$$\frac{d}{dt}(\text{N}_2\text{O}_{atm}) = -Q_{den}^{C:N} \cdot R_{den3}^{atm}. \tag{18d}$$

$$\tag{18e}$$

Descriptions of each nitrogen cycle tracer are presented in Table S5.

December 7, 2022, 8:52pm

S4: Light Inhibition In NitrOMZ, rates of both NH_4^+ and NO_2^- oxidation (R_{ao} and R_{no}, respectively) are photo-inhibited by photosynthetically available radiation (PAR) near the surface, modelled in ROMS-BEC using the same formulation as in Frischknecht et al. (2017). Surface PAR (PAR_{in}) is attenuated with depth via a discretized exponential scale length parameter (λ_{par}) computed from an initial surface value (λ_{par_i}):

$$\lambda_{par_i} = max(0.02, Chl_{tot}), \tag{19}$$

where Chl_{tot} is the sum of community chlorophyll from diatoms (Chl_{diat}), diazotrophs (Chl_{diaz}), and small phytoplankton (Chl_{sp}). The attenuation coefficient is then further modified depending on the initial value of λ_{par_i}:

$$\lambda_{par}(z) = \begin{cases} 0.0919 \cdot (\lambda_{par_i})^{0.3536} \cdot dz & \text{where } \lambda_{par_i} < 0.13224, \\ 0.1131 \cdot (\lambda_{par_i})^{0.4562} \cdot dz & \text{where } \lambda_{par_i} \geq 0.13224. \end{cases} \tag{20}$$

In the initial surface grid cell, attenuation of PAR_{in} from the top of the cell over the cell thickness (m) is calculated as:

$$PAR_{out}(z) = PAR_{in}(z) \cdot e^{-\lambda_{par}(z)}. \tag{21}$$

For each cell, if both $PAR_{in}(z)$ and $PAR_{out}(z)$ are less than the PAR limitation for either rate (PAR_{lim}^{ao} and PAR_{lim}^{no}, here both set to 1 W m^{-2}), then photo-inhibition is avoided and the rates are calculated via equation (11). If only $PAR_{in}(z)$ exceeds PAR limitation, each rate is attenuated via:

$$R_{ao}(z) = R_{ao}(z) \cdot log(\frac{PAR_{out}(z)/PAR_{lim}^{ao}}{-\lambda_{par}(z)}) \tag{22}$$

$$R_{no}(z) = R_{no}(z) \cdot log(\frac{PAR_{out}(z)/PAR_{lim}^{no}}{-\lambda_{par}(z)}). \tag{23}$$

Following the calculation, $PAR_{out}(z)$ is set to $PAR_{in}(z)$ for the cell below and iterated over the number of depths.

December 7, 2022, 8:52pm

Table S1. Organic matter cycle rates.

Rates	Description	Units
$R_{graze,poc}^{sp}$	Grazing loss for small phytoplankton routed to POC	mmol C/m^3/s
$R_{graze,poc}^{diat}$	Grazing loss for diatoms routed to POC	mmol C/m^3/s
$R_{graze,poc}^{diaz}$	Grazing loss for diazotrophs routed to POC	mmol C/m^3/s
R_{agg}^{sp}	Aggregation loss of small phytoplankton	mmol C/m^3/s
R_{agg}^{diat}	Aggregation loss of diatoms	mmol C/m^3/s
R_{agg}^{diaz}	Aggregation loss of diazotrophs	mmol C/m^3/s
$R_{loss,poc}^{sp}$	Non-grazing mortality of small phytoplankton routed to POC	mmol C/m^3/s
$R_{loss,poc}^{diat}$	Non-grazing mortality of diatoms routed to POC	mmol C/m^3/s
$R_{loss,poc}^{diaz}$	Non-grazing mortality of diazotrophs routed to POC	mmol C/m^3/s
R_{poc}^{prod}	Amount of particulate organic C produced	mmol C/m^3/s
$R_{free,poc}^{prod}$	Amount of non-mineral particulate organic C produced	mmol C/m^3/s
$R_{min,poc}^{prod}$	Amount of mineral particulate organic C produced	mmol C/m^3/s
R_{poc}^{rem}	Amount of particulate organic C remineralized	mmol C/m^3/s
Φ_{poc}	Incoming particulate C-flux	mmol C/m^3/s
$\Phi_{free,poc}$	Incoming non-mineral particulate C-flux	mmol C/m^3/s
$\Phi_{min,poc}$	Incoming mineral particulate C-flux	mmol C/m^3/s
Φ_{pcaco3}^{soft}	Incoming soft CaCO$_3$ particulate flux	mmol CaCO$_3$/m^3/s
$\Phi_{psio_2}^{soft}$	Incoming soft SiO$_2$ particulate flux	mmol SiO$_2$/m^3/s
Φ_{dust}^{soft}	Incoming soft dust flux	mmol C/m^3/s
Φ_{pcaco3}^{hard}	Incoming hard CaCO$_3$ particulate flux	mmol CaCO$_3$/m^3/s
$\Phi_{psio_2}^{hard}$	Incoming hard SiO$_2$ particulate flux	mmol SiO$_2$/m^3/s
Φ_{dust}^{hard}	Incoming hard dust flux	mmol C/m^3/s

Table S2. Organic matter cycle parameters

Parameters	Description	Value	Units
ρ_{pcaco3}	Associated molar ratio of $CaCO_3$ to POC	0.417	mol $CaCO_3$ / mol POC
ρ_{psio_2}	Associated molar ratio of SiO_2 to POC	0.250	mol SiO_2 / mol POC
ρ_{dust}	Associated molar ratio of dust to POC	4163.197	mol dust / mol POC
γ_{poc}	Initial length scale for remineralization of POC	88	m
γ_{pcaco3}	Length scale for remineralization of $CaCO_3$	150	m
γ_{psio_2}	Length scale for remineralization of SiO_2	250	m
γ_{dust}	Length scale for remineralization of dust	200	m
λ_{hard}	Length scale for remineralization of hard subclass	40	km
$\lambda_{hard,dust}$	Length scale for remineralization of hard dust subclass	125	km
f_{poc}	Fraction of POC routed to hard subclass	0	N/A
f_{pcaco3}	Fraction of $CaCO_3$ routed to hard subclass	0.3	N/A
f_{psio_2}	Fraction of SiO_2 routed to hard subclass	0.03	N/A
f_{dust}	Fraction of dust routed to hard subclass	0.97	N/A

Table S3. Nitrogen cycle rates

Name	Description	Units
R_{rem}	Remineralized particulate organic C	mmol C/m^3/s
$R_{ao}^{no_2}$	Rate of NH$_4^+$ oxidation to NO$_2^-$	mmol N/m^3/s
$R_{ao}^{n_2o}$	Rate of NH$_4^+$ oxidation to N$_2$O	mmol N/m^3/s
R_{no}	Rate of NO$_2^-$ oxidation to NO$_3^-$	mmol N/m^3/s
R_{den1}	Rate of NO$_3^-$ reduction to NO$_2^-$	mmol C/m^3/s
R_{den2}	Rate of NO$_2^-$ reduction to N$_2$O	mmol C/m^3/s
R_{den3}	Rate of N$_2$O reduction to N_2	mmol C/m^3/s
R_{ax}	Rate of NH$_4^+$ and NO$_2^-$ loss to N_2 via anammox	mmol N/m^3/s
R_{den}^{sed}	Rate of sedimentary denitrification	mmol N/m^3/s
$R_{loss,dic}^{sp}$	Non-grazing mortality of small phytoplankton routed to DIC	mmol C/m^3/s
$R_{loss,dic}^{diat}$	Non-grazing mortality of diatoms routed to DIC	mmol C/m^3/s
$R_{loss,dic}^{diaz}$	Non-grazing mortality of diazotrophs routed to DIC	mmol C/m^3/s
$R_{loss,dic}^{zoo}$	Zooplankton mortality routed to DIC	mmol C/m^3/s
$R_{graze,dic}^{sp}$	Grazed mortality of small phytoplankton routed to DIC	mmol C/m^3/s
$R_{graze,dic}^{diat}$	Grazed mortality of diatoms routed to DIC	mmol C/m^3/s
$R_{graze,dic}^{diaz}$	Grazed mortality of diazotrophs routed to DIC	mmol C/m^3/s
R_{up,nh_4}^{sp}	Uptake of NH$_4^+$ by small phytoplankton	mmol N/m^3/s
R_{up,nh_4}^{diat}	Uptake of NH$_4^+$ by diatoms	mmol N/m^3/s
R_{up,nh_4}^{diaz}	Uptake of NH$_4^+$ by diazotrophs	mmol N/m^3/s
R_{up,no_3}^{sp}	Uptake of NO$_3^-$ by small phytoplankton	mmol N/m^3/s
R_{up,no_3}^{diat}	Uptake of NO$_3^-$ by diatoms	mmol N/m^3/s
R_{up,no_3}^{diaz}	Uptake of NO$_3^-$ by diazotrophs	mmol N/m^3/s
R_{up,no_2}^{sp}	Uptake of NO$_2^-$ by small phytoplankton	mmol N/m^3/s
R_{up,no_2}^{diat}	Uptake of NO$_2^-$ by diatoms	mmol N/m^3/s
R_{up,no_2}^{diaz}	Uptake of NO$_2^-$ by diazotrophs	mmol N/m^3/s

Table S4.   Nitrogen cycle parameters

Parameters	Description	Value	Units
k_{rem}	Maximum respiration rate	9.259E-7	mmol C/m^3/s
k_{ao}	Maximum NH$_4^+$ oxidation rate	5.787E-7	mmol N/m^3/s
k_{no}	Maximum NO$_2^-$ oxidation rate	5.787E-7	mmol N/m^3/s
k_{den1}	Maximum NO$_3^-$ reduction rate	1.852E-7	mmol C/m^3/s
k_{den2}	Maximum NO$_2^-$ reduction rate	9.259E-8	mmol C/m^3/s
k_{den3}	Maximum N$_2$O reduction rate	5.741E-7	mmol C/m^3/s
k_{ax}	Maximum anaerobic NH$_4^+$ oxidation rate	5.105E-6	mmol N/m^3/s
$K_{rem}^{o_2}$	Respiration half-saturation constant for O$_2$ uptake	1.000	mmol O$_2$/m^3
$K_{ao}^{o_2}$	NH$_4^+$ oxidation half-saturation constant for O$_2$ uptake	0.333	mmol N/m^3
$K_{ao}^{nh_4}$	NH$_4^+$ oxidation half-saturation constant for NH$_4^+$ uptake	0.305	mmol N/m^3
$K_{no}^{o_2}$	NO$_2^-$ oxidation half-saturation constant for O$_2$ uptake	0.778	mmol N/m^3
$K_{no}^{no_2}$	NO$_2^-$ oxidation half-saturation constant for NO$_2^-$ uptake	0.509	mmol N/m^3
$K_{den1}^{no_3}$	NO$_3^-$ reduction half-saturation constant for NO$_3^-$ uptake	1.000	mmol N/m^3
$K_{den2}^{no_2}$	NO$_2^-$ reduction half-saturation constant for NO$_2^-$ uptake	0.010	mmol N/m^3
$K_{den3}^{n_2o}$	N$_2$O reduction half-saturation constant for N$_2$O uptake	0.159	mmol N/m^3
$K_{ax}^{nh_4}$	NH$_4^+$ oxidation half-saturation constant for NH$_4^+$ uptake	0.230	mmol N/m^3
$K_{ax}^{no_2}$	NH$_4^+$ oxidation half-saturation constant for NO$_2^-$ uptake	0.100	mmol N/m^3
a	O$_2$-dependent coefficient (Nevison et al., 2003)	0.300	N/A
b	Background coefficient (Nevison et al., 2003)	0.100	N/A
$K_{den1}^{o_2}$	O$_2$ poisoning constant for NO$_3^-$ reduction	6.000	mmol O$_2$/m^3
$K_{den2}^{o_2}$	O$_2$ poisoning constant for NO$_2^-$ reduction	2.300	mmol O$_2$/m^3
$K_{den3}^{o_2}$	O$_2$ poisoning constant for N$_2$O reduction	0.506	mmol O$_2$/m^3
$K_{ax}^{o_2}$	O$_2$ poisoning constant for anammox	6.000	mmol O$_2$/m^3
τ^{DON}	Semi-labile DON remineralization inverse timescale	1.826E-4	1/s
τ^{DONr}	Refractory DON remineralization inverse timescale	2.884E-7	1/s
Q^{DONr}	Fraction of DON to refractory pool	0.0115	N/A
PAR_{lim}^{ao}	PAR limitation for NH$_4^+$ oxidation	1.000	W/m^2
PAR_{lim}^{no}	PAR limitation for NO$_2^-$ oxidation	1.000	W/m^2

Table S5. Nitrogen cycle tracers

Name	Description	Units
DON	Dissolved organic nitrogen	mmol N/m^3
DONr	Refractory dissolved organic nitrogen	mmol N/m^3
NH_4^+	Ammonium	mmol N/m^3
NO_2^-	Nitrite	mmol N/m^3
NO_3^-	Nitrate	mmol N/m^3
N_2O	Nitrous oxide	mmol N/m^3
N_2O_{den}	Nitrous oxide sourced from denitrification	mmol N/m^3
N_2O_{nit}	Nitrous oxide sourced from nitrification	mmol N/m^3
N_2O_{atm}	Saturated nitrous oxide sourced from boundaries and ingassing	mmol N/m^3
N_2O_{bou}	Supersaturated nitrous oxide sourced from boundaries	mmol N/m^3
N_2	Dinitrogen	mmol N/m^3
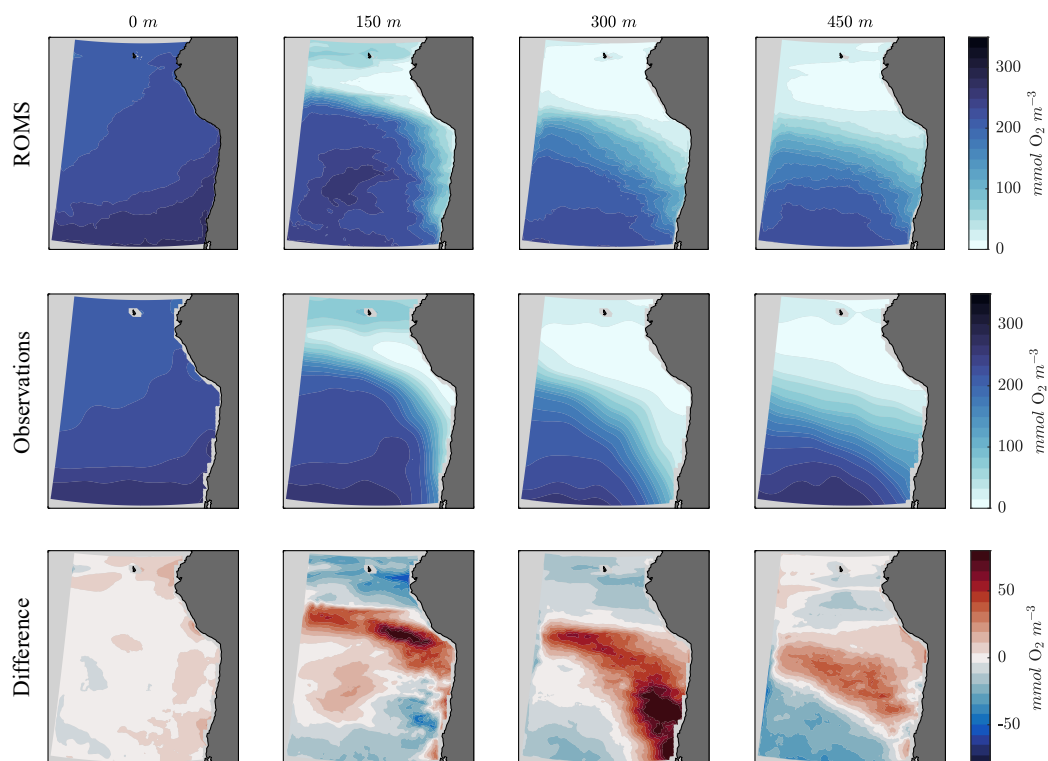
Figure S1.   0, 150, 300, and 450 m annually averaged O_2 from (top) ROMS model years 46 - 50, (middle) World Ocean Atlas 2018 O_2 (Garcia et al., 2019), and (bottom) their differences (ROMS - WOA18).

December 7, 2022, 8:52pm
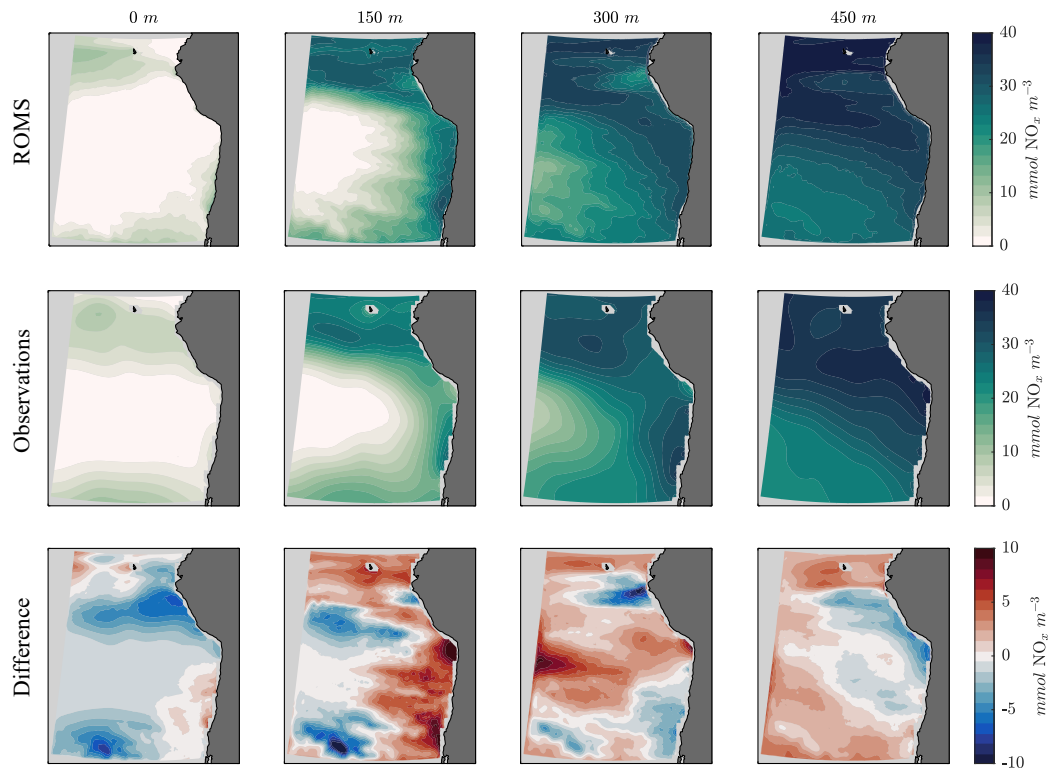
Figure S2.   Same as in Figure S1, but for nitrate + nitrite (NO$_x$).
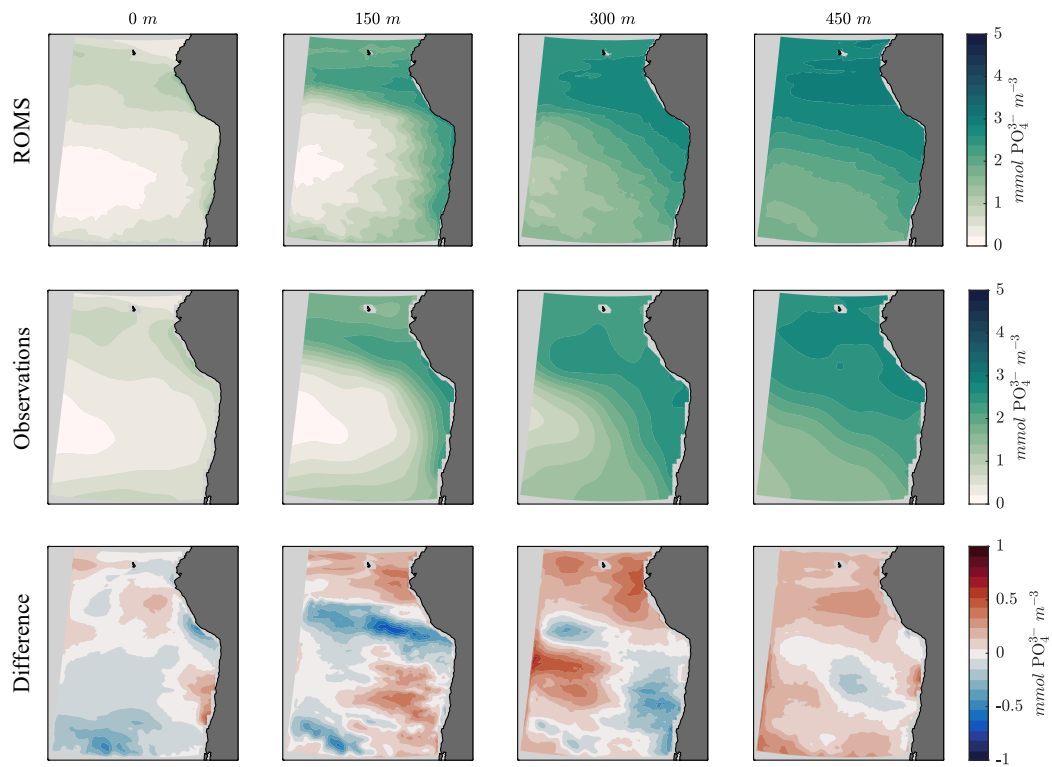
Figure S3.   Same as in Figure S1, but for phosphate (PO_4^{3-}).
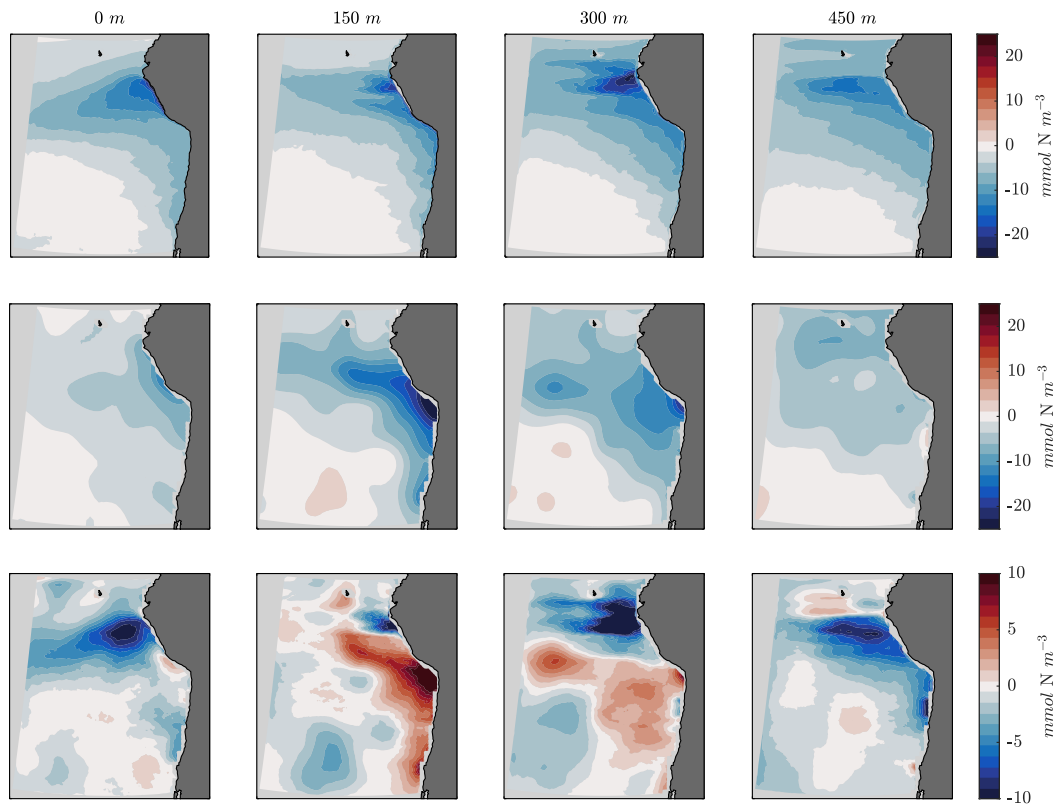
Figure S4. Same as in Figure S1, but for N* (here defined as $16 \cdot [\text{NO}_3^-]$ - $[\text{PO}_4^{3-}]$).
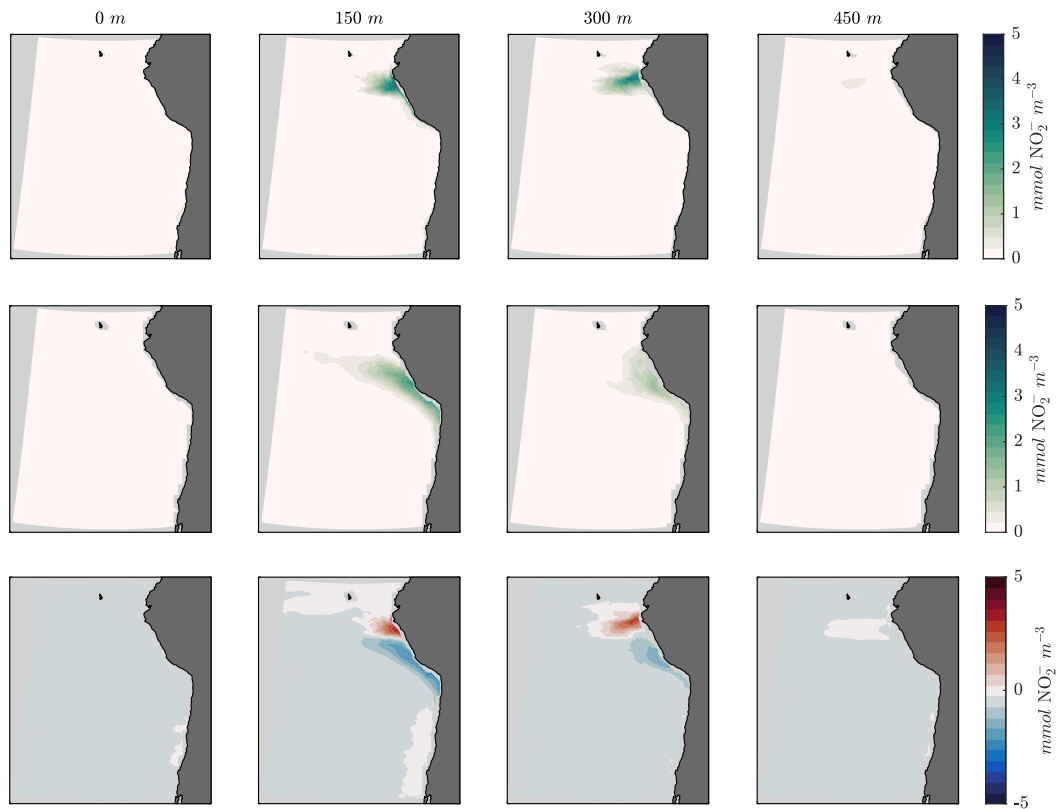
Figure S5. Same as in Figure S1, but for NO_2^- comparisons against machine learning estimates.
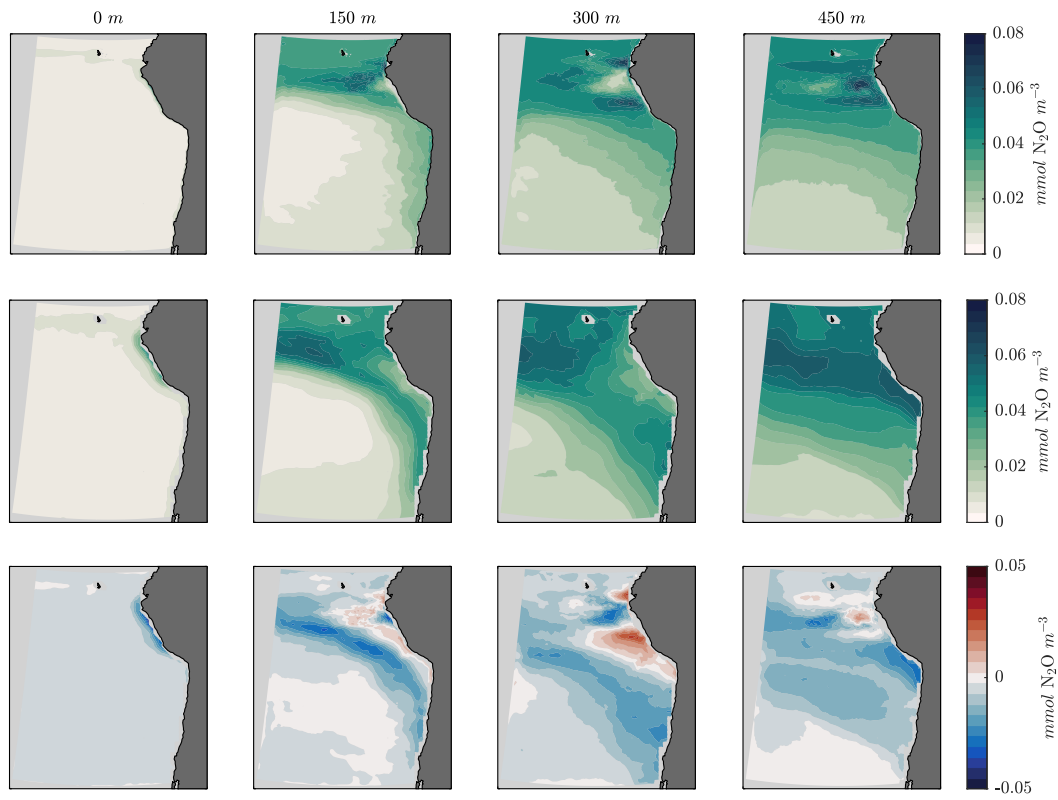
Figure S6. Same as in Figure S1, but for N_2O comparisons against machine learning estimates.

December 7, 2022, 8:52pm
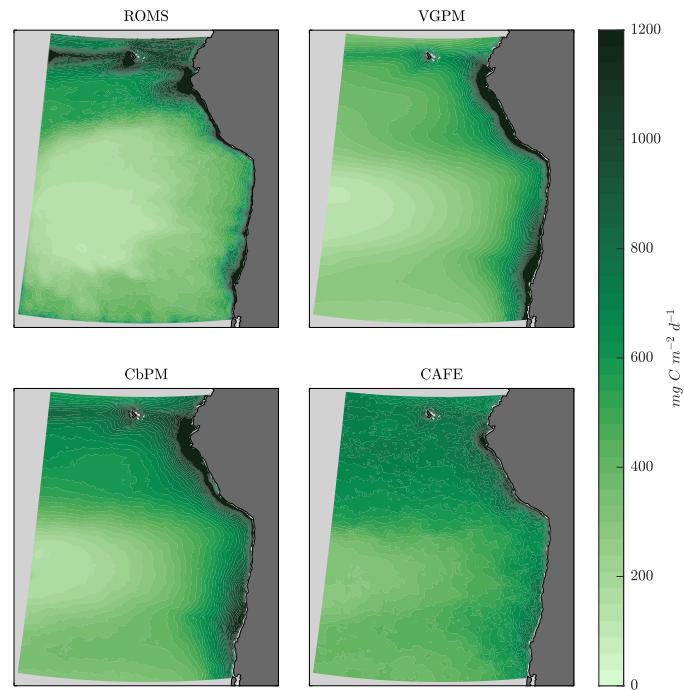
Figure S7. Annually averaged net Primary Production (NPP) from (top left) ROMS model years 46 - 50, (top right) the Eppley Vertically Generalized Production Model (Eppley-VGPM, Behrenfeld and Falkowski (1997))), (bottom left) the updated Carbon-Based Productivity Model (CbPM, Behrenfeld et al. (2005)), and (bottom right) the Fluorescence Euphotic-resolving model (CAFE, Silsbe et al. (2016)).
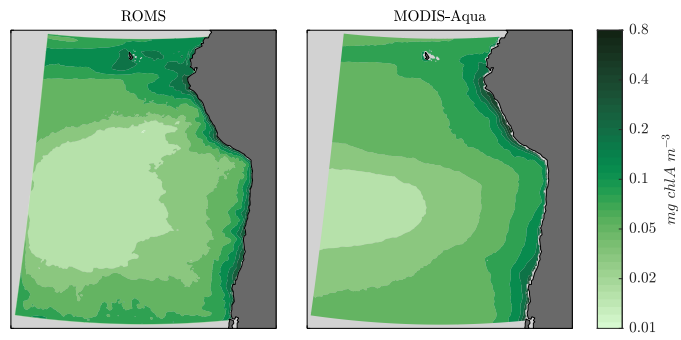
Figure S8. Annually averaged surface chlorophyll-A (chlA) from (left) ROMS model years 46 - 50 and (right) MODIS-Aqua.
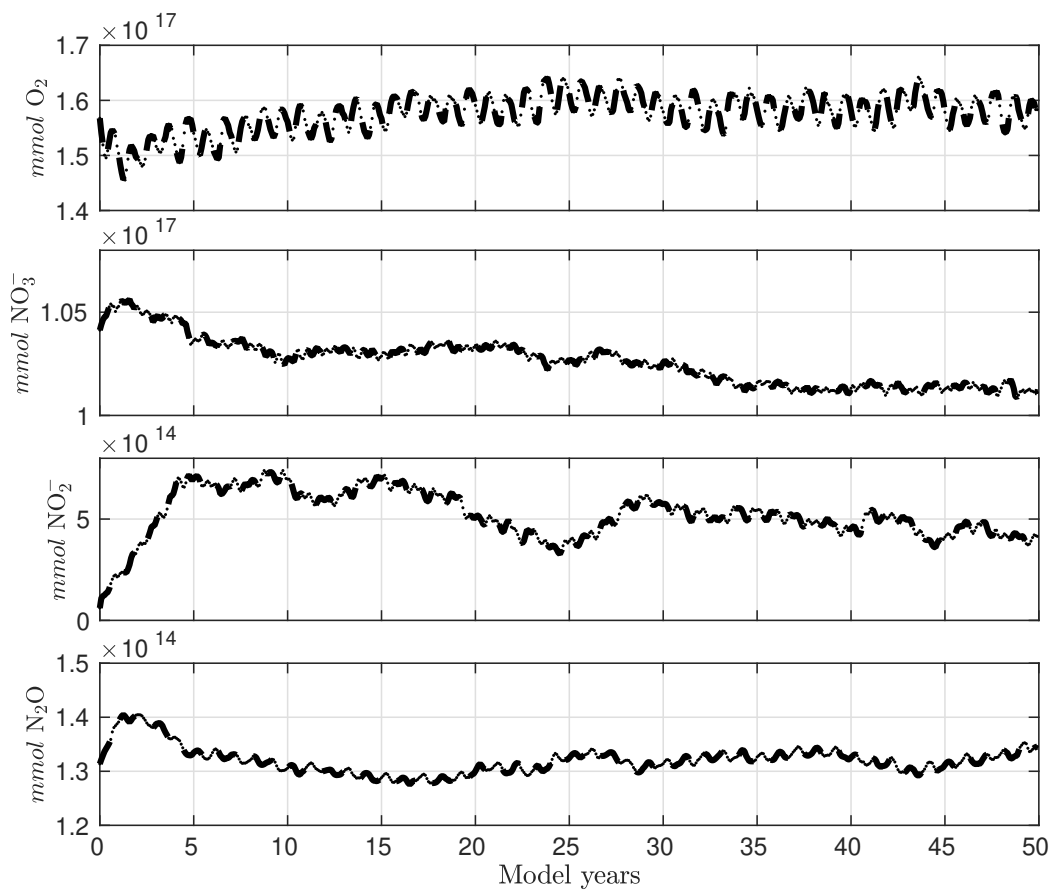
Figure S9.   Integrated O_2, NO_3^-, NO_2^-, and N_2O tracers within the OMZ budget domain for model years 0 - 50.
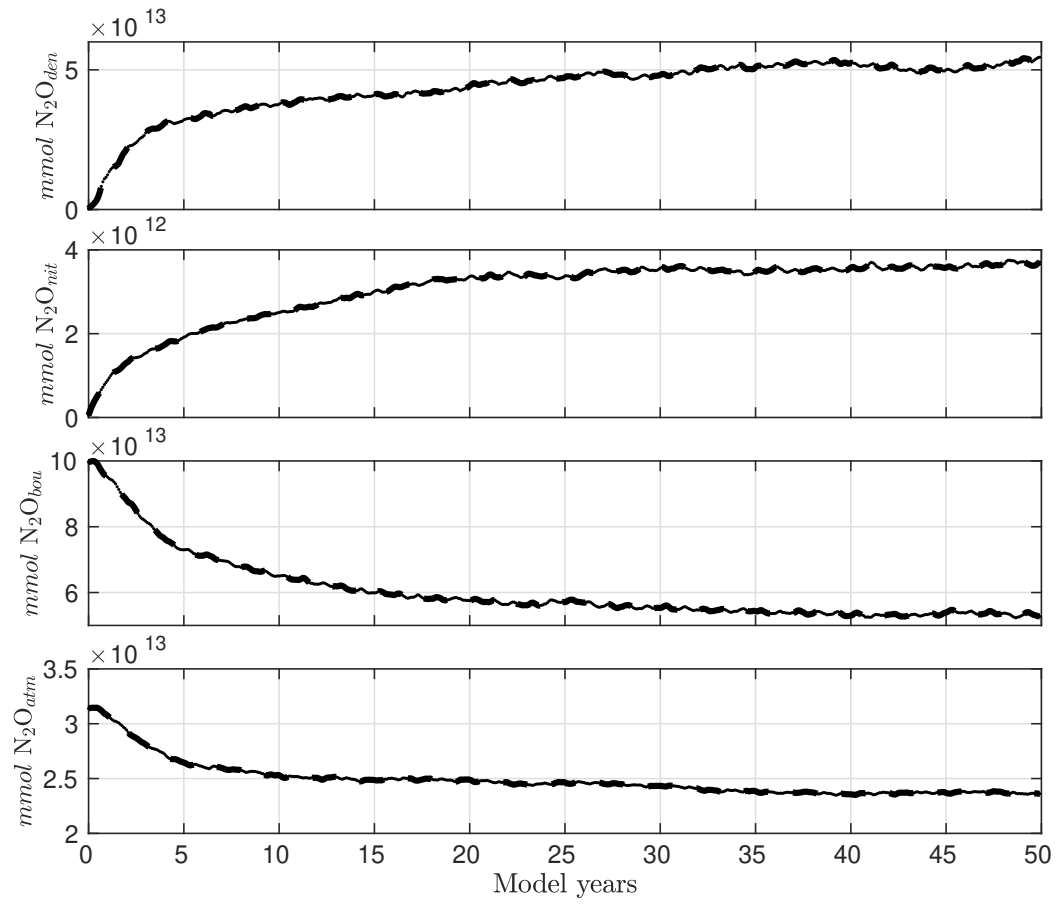
Figure S10. Integrated N_2O_{nit}, N_2O_{den}, N_2O_{bou}, and N_2O_{atm} tracers within the OMZ budget domain for model years 0 - 50.
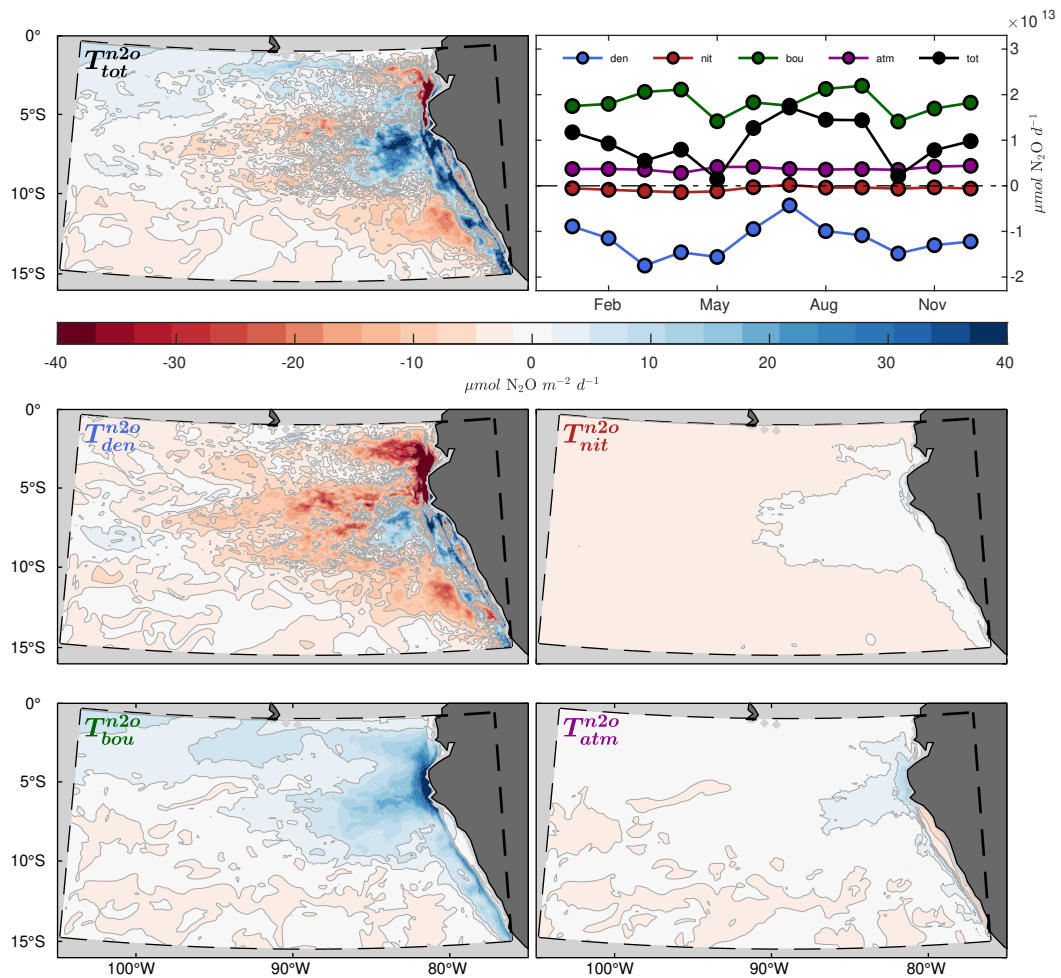
Figure S11. (top left) Vertically integrated divergence of advective and diffusive fluxes (T) for N_2O from the OMZ budget domain, annually averaged from model years 46 - 50. (top right) Time-series of integrated divergence of advective and diffusive fluxes for N_2O (black) and the decomposed N_2O tracers. (bottom panels) Same as in the top left panel, but for each of the decomposed N_2O tracers. Positive values are shown in blue, and negative values in red.

December 7, 2022, 8:52pm
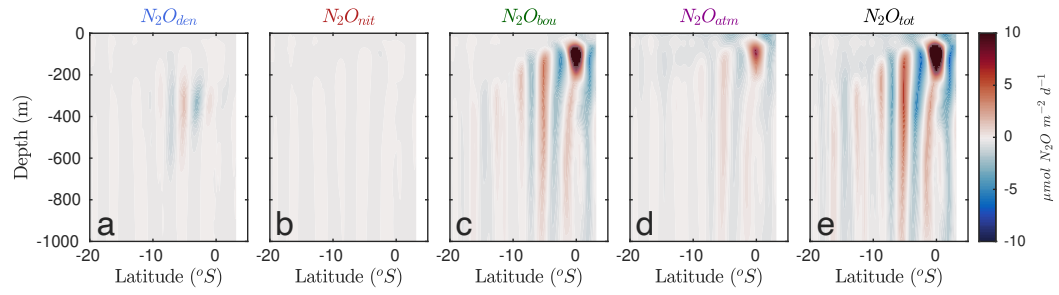
Figure S12. Annually averaged zonal N_2O transport from the western boundary of the OMZ budget domain (roughly 105^oW) from model years 46 - 50 for (a) N_2O_{den}, (b) N_2O_{nit}, (c) N_2O_{bou}, (d) N_2O_{atm}, and (e) N_2O.
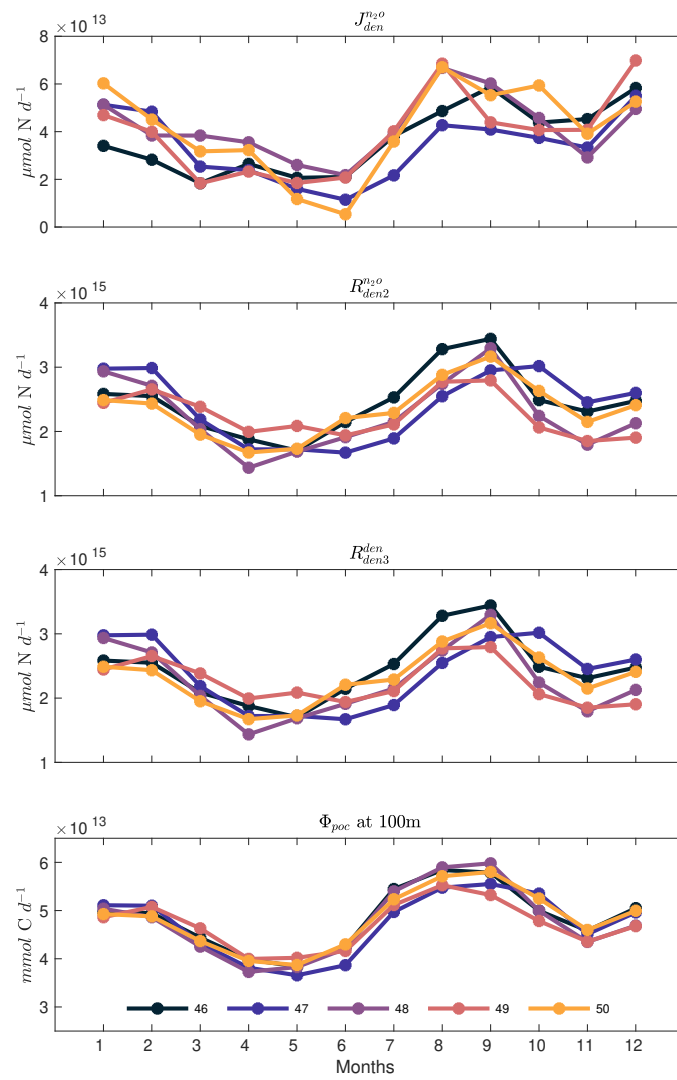
Figure S13. Integrated net N$_2$O production rate from denitrification (J_{den}^{n2o}), integrated NO$_2^-$ reduction rate (R_{den2}^{n2o}), integrated N$_2$O reduction rate of denitrification-sourced N$_2$O (R_{den}^{den3}), and vertical POC flux (Φ_{poc}) at 100m from the OMZ budget domain for ROMS model years 46 - 50.
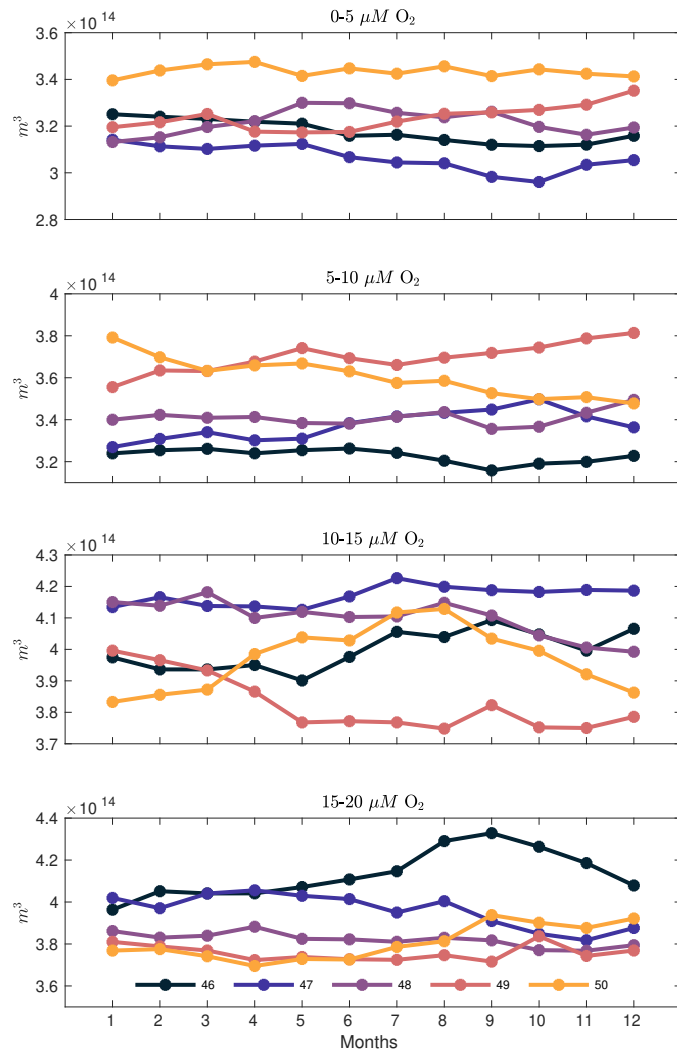
Figure S14. Volume of the OMZ budget domain occupied by various O_2 thresholds (0 - 5, 5 - 10, 10 - 15, and 15 - 20 $mmol$ O_2 m^{-3}) for ROMS model years 46 - 50.

References

Anderson, L. A., & Sarmiento, J. L. (1994, 3). Redfield ratios of remineralization determined by nutrient data analysis. *Global Biogeochemical Cycles*, *8*(1), 65–80. Retrieved from `http://doi.wiley.com/10.1029/93GB03318` doi: 10.1029/93GB03318

Armstrong, R. A., Lee, C., Hedges, J. I., Honjo, S., & Wakeham, S. G. (2001, 1). A new, mechanistic model for organic carbon fluxes in the ocean based on the quantitative association of POC with ballast minerals. *Deep Sea Research Part II: Topical Studies in Oceanography*, *49*(1-3), 219–236. Retrieved from `https://linkinghub.elsevier.com/retrieve/pii/S0967064501001011` doi: 10.1016/S0967-0645(01)00101-1

Behrenfeld, M. J., Boss, E., Siegel, D. A., & Shea, D. M. (2005, 3). Carbon-based ocean productivity and phytoplankton physiology from space. *Global Biogeochemical Cycles*, *19*(1). Retrieved from `http://doi.wiley.com/10.1029/2004GB002299` doi: 10.1029/2004GB002299

Behrenfeld, M. J., & Falkowski, P. G. (1997, 1). Photosynthetic rates derived from satellite-based chlorophyll concentration. *Limnology and Oceanography*, *42*(1), 1–20. Retrieved from `http://doi.wiley.com/10.4319/lo.1997.42.1.0001` doi: 10.4319/lo.1997.42.1.0001

Bianchi, D., McCoy, D., & Yang, S. (2022). Formulation, optimization and sensitivity of nitromzv1.0, a biogeochemical model of the nitrogen cycle in oceanic oxygen minimum zones. *Geoscientific Model Development Discussions*. doi: 10.5194/gmd-2022-244

Deutsch, C., Frenzel, H., McWilliams, J. C., Renault, L., Kessouri, F., Howard, E., . . . Yang, S. (2021). Biogeochemical variability in the california current system. *Progress in Oceanography*, *196*, 102565. Retrieved from `https://www.sciencedirect.com/science/article/pii/S0079661121000525` doi: https://doi.org/10.1016/j.pocean.2021.102565

Frischknecht, M., Münnich, M., & Gruber, N. (2017, 1). Local atmospheric forcing driving an unexpected California Current System response during the 2015–2016 El Niño. *Geophysical Research Letters*, *44*(1), 304–311. doi: 10.1002/2016GL071316

Garcia, H., Weathers, K., Paver, C., Smolyar, I., Boyer, T., Locarnini, M., . . . Reagan, J. (2019). World Ocean Atlas 2018, Volume 3: Dissolved Oxygen, Apparent Oxygen Utilization, and Dissolved Oxygen Saturation. *NOAA Atlas NESDIS*, *83*.

Moore, J. K., Doney, S. C., & Lindsay, K. (2004, 12). Upper ocean ecosystem dynamics and iron cycling in a global three-dimensional model. *Global Biogeochemical Cycles*, *18*(4), n/a-n/a. Retrieved from `http://doi.wiley.com/10.1029/2004GB002220` doi: 10.1029/2004GB002220

Silsbe, G. M., Behrenfeld, M. J., Halsey, K. H., Milligan, A. J., & Westberry, T. K. (2016, 12). The CAFE model: A net production model for global ocean phytoplankton. *Global Biogeochemical Cycles*, *30*(12), 1756–1777. Retrieved from `http://doi.wiley.com/10.1002/2016GB005521` doi: 10.1002/2016GB005521